

Low-Noise Amplifier Design for Ultrawideband Radio

Jongrit Lerdworatawee, *Student Member, IEEE*, and Won Namgoong, *Member, IEEE*

Abstract—A new theoretical approach for designing a low-noise amplifier (LNA) for the ultra-wideband (UWB) radio is presented. Unlike narrow-band systems, the use of the noise figure (NF) performance metric becomes problematic in UWB systems because of the difficulty in defining the signal-to-noise ratio (SNR). By defining the SNR as the matched filter bound (MFB), the NF measures the degree of degradation caused by the LNA in the achievable receiver performance after the digital decoding process. The optimum noise matching network that minimizes the NF as defined above has been solved. When the narrow-band LNA assumption is made, the proposed optimum matching network simplifies to the published optimum narrow-band matching network, and the corresponding NF value also becomes equivalent. Since realizing the optimum matching network is in general difficult, an approach for designing a practical but suboptimum matching network is also presented.

Index Terms—Circuit analysis, circuit optimization, CMOS analog integrated circuits, integrated circuit noise, MOSFET amplifiers.

I. INTRODUCTION

THE ultrawideband (UWB) radio is a relatively new technology that is being pursued for both commercial and military purposes [1]–[3]. The rationale for deploying the UWB radio systems lies in the benefits of exceptionally wide bandwidths in very low frequency ranges, thereby achieving a combination of very fine time/range resolution, ability to resolve multipath components, and favorable propagation condition of material penetration at low frequencies [4], [5].

The UWB radio operates by spreading the energy of the radio signal very thinly from near d.c. to a few gigahertz. Since this frequency range is highly populated, the UWB radio must contend with a variety of interfering signals, and it must not interfere with narrow-band radio systems operating in dedicated bands. These requirements necessitate the use of spread spectrum techniques. Both time-hopping and direct-sequence spread spectrum UWB systems have been studied.

The goal of the receiver analog front-end is to condition the received analog signal for digitization, so that the highest per-

formance can be achieved after decoding in the digital domain. The first and probably the most critical component of the analog front-end is the low-noise amplifier (LNA), whose purpose is to amplify the received signal from the antenna with as little distortion and additional noise as possible. This is achieved by designing an appropriate matching network placed before the amplifier as shown in Fig. 1(a).

Although great headway has recently been made in efficient implementation of narrow-band LNA [6], the LNA design requirements for an UWB radio differs fundamentally. Unlike the narrow-band LNA, the signal bandwidth of an UWB radio is several orders of magnitude greater. Hence, the underlying signal-tone signal assumption employed in narrow-band LNA design becomes invalid, making many of the existing narrow-band design techniques based on this assumption also unsuitable.

The metric generally employed to quantify the performance of the LNA is the noise factor [or noise figure (NF) in decibels], which is defined as the ratio of the signal-to-noise ratio (SNR) at the input of the LNA to the SNR at the output of the LNA [7], [8]. Although the use of the NF metric is straightforward in narrow-band systems, its use becomes more difficult in UWB systems. The main difficulty arises in defining the SNR. In a narrow-band system, where both the input signal and noise are assumed to be a single tone at the carrier frequency, the SNR is obtained by simply dividing the signal power by the noise power. In an UWB system, however, the input signal is broadband and the additive noise may be colored. The SNR obtained by simply dividing the signal power by the total noise power (whose bandwidth must also be defined) is less meaningful, since a higher SNR value defined in this manner does not necessarily translate to a higher receiver performance. This is because the performance of the receiver after the digital decoding process does not depend on the total signal and noise power but on the power-spectral density (PSD) of the additive noise and the impulse responses of the propagation channel and the transmit pulse.

Because of the difficulty in defining the SNR, existing work on broadband matching defines the NF as a linearly weighted average of the single-tone NF [7]. Although such a definition of NF is a straightforward extension of a single-tone NF and can be easily computed, minimizing such arbitrary performance metric does not necessarily improve the overall receiver performance.

For the NF of the LNA to be a meaningful metric in an UWB receiver, the SNR at the input and output of the LNA should measure the achievable performance after the eventual digital decoding process, as it is ultimately the most relevant measure of performance. Hence, we define the SNR as the matched filter

Manuscript received May 12, 2003; revised August 31, 2003. This work was supported in part by the Army Research Office under Contract DAAD19-01-1-0477 and in part by the National Science Foundation under Contract ECS-0134629. This paper was recommended by Associate Editor A. I. Karsilayan.

J. Lerdworatawee is with the Department of Electrical Engineering, University of Southern California, Los Angeles, CA 90089 USA (e-mail: lerdwora@usc.edu).

W. Namgoong is with the Department of Electrical Engineering Systems, University of Southern California, Los Angeles, CA 90089-2562 USA (e-mail: namgoong@usc.edu).

Digital Object Identifier 10.1109/TCSI.2004.829305

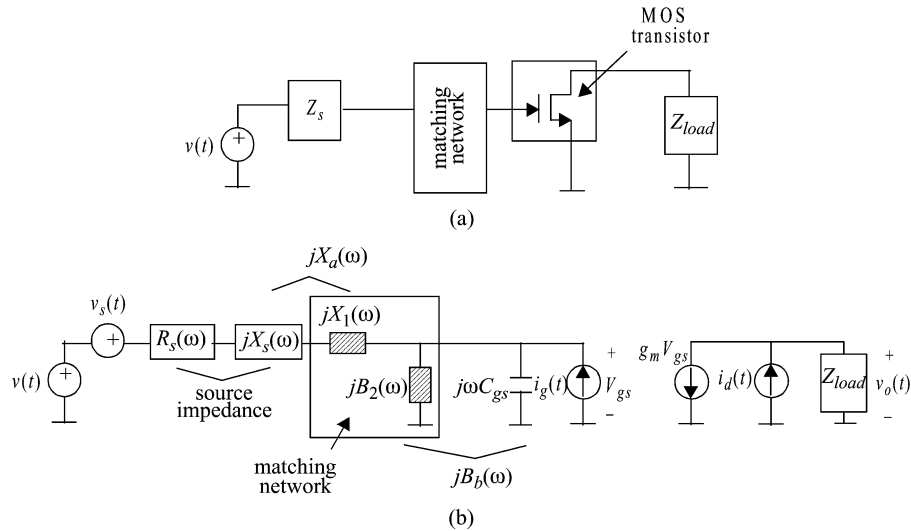


Fig. 1. General model of LNA. (a) Block diagram of LNA. (b) Equivalent circuit model.

bound (MFB) [9], which represents an upper limit on the performance of data transmission systems. The MFB is obtained when a noise whitened matched filter is employed to receive a single transmitted pulse. By defining the SNR as the MFB, the NF measures the degree of degradation in the achievable receiver performance caused by the LNA.

This paper solves the optimum matching network that minimizes the NF with the SNR defined as the MFB. When the input is assumed to be a single tone, the optimum NF equation converges to the existing minimum NF derivation for a narrow-band LNA. The optimum matching network, however, requires arbitrary reactance values that may be difficult to realize. Therefore, a suboptimum matching network that approximates the optimum matching network can be used. An approach for designing the suboptimum matching network using numerical optimization technique is described. The performance of both the optimum and suboptimum matching network is then studied for different LNA gain and received signal bandwidth. The effect of narrow-band interferers is also addressed.

The organization of the paper is as follows. The circuit and system model of the LNA is presented in Section II. In Section III, the general solution to the matching network for optimal LNA is derived. As this optimal LNA matching is, in general, not practical, a suboptimal LNA matching technique is presented by solving a constrained optimization problem as described in Section IV. The performance results are presented in Section V. Conclusions are drawn in Section VI.

II. CIRCUIT AND SYSTEM MODEL

Throughout this paper, capital letters are used to denote the Fourier transforms [e.g., $X(\omega)$] of (voltage or current) system responses in the time domain, which are written in the corresponding lower case letters [e.g., $x(t)$]. Sometimes the terms ω and t are omitted for notational brevity unless needed for clarity.

A. MOS Transistor Model

This section describes the transistor model used in this paper. The quasi-static MOS transistor model is employed to account

for the high-field effects in short-channel devices. The drain current I_d is [8], [10]

$$I_d = \begin{cases} 2v_{\text{sat}}C_{\text{ox}}W \frac{(V_{\text{od}} - V_{\text{ds}}/2)V_{\text{ds}}}{(V_{\text{ds}} + L\varepsilon_{\text{sat}})}, & V_{\text{ds}} \leq V_{\text{dsat}} \\ v_{\text{sat}}C_{\text{ox}}W \frac{V_{\text{od}}^2}{V_{\text{od}} + L\varepsilon_{\text{sat}}}, & V_{\text{ds}} \geq V_{\text{dsat}} \end{cases} \quad (1)$$

where W and L are the gate width and length, and C_{ox} is the gate-oxide capacitance per unit area. The gate overdrive V_{od} , the effective electron mobility μ_{eff} , and the saturation velocity v_{sat} are

$$V_{\text{od}} = V_{\text{gs}} - V_{\text{th}} \quad (2)$$

$$\mu_{\text{eff}} = \frac{\mu_n}{1 + V_{\text{od}}/L\varepsilon_{\text{sat}}} \quad (3)$$

$$v_{\text{sat}} = \mu_n \varepsilon_{\text{sat}}/2 \quad (4)$$

where V_{gs} is the gate-source voltage, V_{th} is the threshold voltage, μ_n is the electron mobility, and ε_{sat} is the saturation electric field. In (1), V_{ds} is the drain-source voltage and V_{dsat} is the drain-source saturation voltage, which is given by

$$V_{\text{dsat}} = \frac{V_{\text{od}}}{V_{\text{od}} + L\varepsilon_{\text{sat}}}. \quad (5)$$

Since W is fixed (assuming minimum length) when V_{od} and I_d are specified, the transconductance g_m , the zero-bias drain conductance g_{d0} , and the gate-source capacitance $C_{\text{gs}}(=2WLC_{\text{ox}}/3)$ can be represented in terms of the normalized gate overdrive $\rho(=V_{\text{od}}/L\varepsilon_{\text{sat}})$ and power dissipation $P_o(=I_dV_{\text{supply}})$

$$g_m = \frac{2P_o}{V_{\text{dd}}L\varepsilon_{\text{sat}}} \left[\frac{1 + \rho/2}{\rho(1 + \rho)} \right] \quad (6)$$

$$g_{d0} = \frac{2P_o}{V_{\text{dd}}L\varepsilon_{\text{sat}}} \left[\frac{1 + \rho}{\rho} \right] \quad (7)$$

$$C_{\text{gs}} = \frac{2}{3} \frac{P_o}{V_{\text{dd}}v_{\text{sat}}\varepsilon_{\text{sat}}} \left(\frac{1 + \rho}{\rho^2} \right). \quad (8)$$

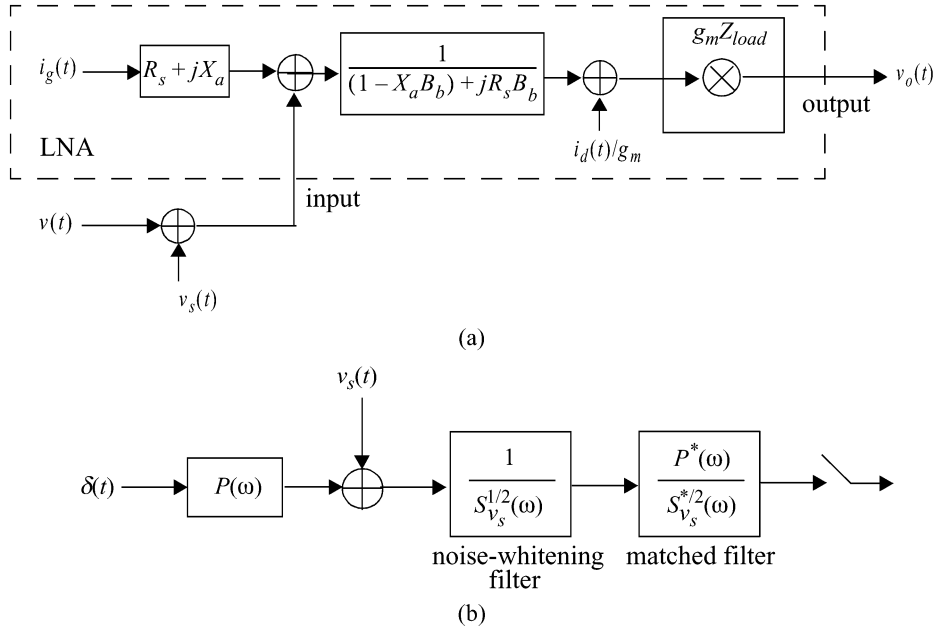


Fig. 2. Overall system model. (a) System model of LNA. (b) MFB computation at the input of LNA.

B. Circuit Model of LNA

A block diagram of the LNA is shown in Fig. 1(a). The LNA consists of three components: a matching network, an amplifier, and a load. The amplifier is assumed to be a MOS transistor with a common-source configuration. Fig. 1(b) is the circuit model of Fig. 1(a). The received UWB signal is represented as a voltage generator $v(t)$ and $Z_s(\omega) = R_s(\omega) + jX_s(\omega)$ is the corresponding source impedance. The MOS transistor is modeled by gate-source capacitance C_{gs} , a voltage-to-current converter $g_m V_{gs}$, and two current noise sources $i_g(t)$ and $i_d(t)$. The matching network is assumed lossless, consisting of reactance $X_1(\omega)$ and susceptance $B_2(\omega)$, as illustrated by the dash-line block in Fig. 1(b). For ease of analysis, the source reactance $X_s(\omega)$ is grouped with $X_1(\omega)$ and referred to as $X_a(\omega)$, and the gate-source capacitance C_{gs} is grouped with $B_2(\omega)$ and referred to as $B_b(\omega)$.

In Fig. 1(b), there exists three noise sources: the received voltage noise $v_s(t)$ (i.e., consisting of the thermal noise and the narrow-band interference), the MOS drain current noise $i_d(t)$, and the induced gate current noise $i_g(t)$. Their PSDs are given by [11]–[17]

$$S_{v_s}(\omega) = 4kTR_S(\omega) + S_I(\omega) \quad (9)$$

$$S_{i_d}(\omega) = 4kT\gamma g_{d0} \quad (10)$$

$$S_{i_g}(\omega) = 4kT\delta \frac{(\omega C_{gs})^2}{5g_{d0}} \quad (11)$$

where $k = 1.38 \times 10^{-23}$ J/K is the Boltzmann constant, T is the absolute temperature, $S_I(\omega)$ is the PSD of the narrow-band interferer, and γ and δ are the coefficients of channel and induced gate noise. In (9), the first term on the right-hand side is the input thermal noise and the second term is the received interference noise (i.e., narrow-band interferer). When computing the NF, $S_{v_s}(\omega)$ is assumed by definition to consist only of the

input thermal noise with noise temperature of 290 K. The interference term $S_I(\omega)$ is considered when studying the effect of narrow-band interferer on the LNA design in a later section.

The random noise processes $i_g(t)$ and $i_d(t)$ are correlated with correlation coefficient c given by [15]

$$c = \frac{S_{i_g i_d}(\omega)}{\sqrt{S_{i_g}(\omega)} \cdot \sqrt{S_{i_d}(\omega)}} \quad (12)$$

where $S_{i_g i_d}(\omega)$ is the PSD of the cross-correlation of $i_g(t)$ and $i_d(t)$. For a long-channel transistor, γ , δ , and c are classically equal to $2/3$, $4/3$, and $j0.394$, respectively, but they are higher for a short-channel transistor.

C. System Model of LNA

Fig. 2(a) is the system model of the circuit model in Fig. 1(b). The objective is to design the causal matching network [i.e., reactance $X_a(\omega)$ and susceptance $B_b(\omega)$] so that the SNR of the output voltage $v_o(t)$ is maximized. The voltage amplification of the received voltage signal $v(t)$ is achieved in two stages by the matching network and the transistor. In the absence of the induced gate noise $i_g(t)$, the highest output SNR is obtained by maximizing the gain in the matching network so that the effect of the drain noise is minimized. This is achieved by setting $X_a(\omega) = 1/B_b(\omega)$ and making $|X_a(\omega)|$ as large as possible. In the narrow-band system, such matching is equivalent to simply tuning the matching network to resonate at the carrier frequency. In the realistic case with the induced gate noise $i_g(t)$ present, however, increasing the gain in the matching network too much reduces the output SNR as $i_g(t)$ is also amplified. Hence, there is an optimum gain in the matching network that balances the combined effects of $i_g(t)$ with signal amplification. The matching network should also exploit the correlation between $i_g(t)$ and $i_d(t)$ to reduce the total noise at the output.

For ease of analysis, the induced gate noise $i_g(t)$ is decomposed into two orthogonal components, i.e.,

$$i_g(t) = i_{\text{gu}}(t) + y_c(t) \otimes \frac{i_d(t)}{g_m} \quad (13)$$

where \otimes is the convolution operator, $i_{\text{gu}}(t)$ is the component of $i_g(t)$ that is uncorrelated to $i_d(t)$, and $y_c(t)$ is the equivalent correlation admittance between $i_g(t)$ and $i_d(t)/g_m$. Premultiplying both sides of (13) by $i_d^*(t-\tau)$ followed by the expectation operation, the Fourier transform of the correlation admittance $Y_c(\omega)$ can be obtained and given by

$$\begin{aligned} Y_c(\omega) &= g_m \frac{S_{i_g i_d}(\omega)}{S_{i_d}(\omega)} \\ &= j\omega C_{\text{gs}} \cdot \left\{ \frac{g_m}{g_{d0}} |c| \sqrt{\frac{\delta}{5\gamma}} \right\} \\ &\triangleq jB_c(\omega). \end{aligned} \quad (14)$$

The second equality in (14) is obtained by using (10)–(12).

D. Matched Filter Bound

The MFB, also called the “one-shot” bound, is an upper limit on the performance of data transmission systems with inter-symbol interference (ISI) [9]. As an example, the computation of the MFB at the input of the LNA is illustrated in Fig. 2(b). An impulse is transmitted through the equivalent pulse response $P(\omega)$, which represents the combination of both the transmitted pulse and the propagation channel. After being corrupted by $v_s(t)$, the resulting signal is the input to the LNA. To compute the MFB at this point, the input to the LNA is noise whitened followed by a matched filter that is matched to both the pulse response and the noise whitening filter. The matched filter output is then sampled when the signal is at its maximum. The resulting SNR is the MFB.

Using the MFB definition of the SNR, the SNR at the input of the LNA (i.e., the SNR of the received input signal) is given by

$$\text{SNR}_{\text{in}} = \int_{-\infty}^{\infty} \frac{|P(\omega)|^2}{S_{v_s}(\omega)} d\omega. \quad (15)$$

Similarly, the SNR at the output of the LNA is

$$\text{SNR}_{\text{out}} = \int_{-\infty}^{\infty} \frac{|P(\omega)|^2}{S_{v_s}(\omega) + S_{v_{\text{ir}}}(\omega)} d\omega. \quad (16)$$

In (16), $S_{v_{\text{ir}}}(\omega)$ represents the input-referred noise PSD of all the internally generated noise sources to the gate of the LNA, which is given by

$$\begin{aligned} S_{v_{\text{ir}}} &= S_{i_{\text{gu}}} (R_s^2 + X_a^2) + [R_s^2 (B_b + B_c)^2 \\ &\quad + (1 - X_a (B_b + B_c))^2] \frac{S_{i_d}}{g_m^2} \end{aligned} \quad (17)$$

where the spectrum of the uncorrelated gate noise ($i_{\text{gu}}(t)$) is

$$S_{i_{\text{gu}}}(\omega) = 4kT\delta \frac{(\omega C_{\text{gs}})^2}{5g_{d0}} (1 - |c|^2). \quad (18)$$

Since the SNR_{in} is unaffected by the LNA matching network, minimizing the NF is equivalent to maximizing the SNR_{out} given in (16). Hence, the objective in designing the LNA

matching network is to design $X_a(\omega)$ and $B_b(\omega)$ so that SNR_{out} is maximized.

III. OPTIMAL LNA MATCHING

Reactance $X_a(\omega)$ and susceptance $B_b(\omega)$ that maximize SNR_{out} are obtained by differentiating the indefinite integral in (16) with respect to $X_a(\omega)$ and $B_b(\omega)$, setting the result to zero, and solving for $X_a(\omega)$ and $B_b(\omega)$. Depending on the operating conditions, two possible results can be obtained. First, if $S_{i_{\text{gu}}}(\omega)R_s^2(\omega)g_m^2 \geq S_{i_d}(\omega)$, the optimum $X_a(\omega)$ and $B_b(\omega)$, denoted as $X_{a,\text{opt}}(\omega)$ and $B_{b,\text{opt}}(\omega)$, are given by

$$X_{a,\text{opt}}(\omega) = 0, \quad (19)$$

$$B_{b,\text{opt}}(\omega) = -B_c(\omega). \quad (20)$$

Second, if $S_{i_{\text{gu}}}(\omega)R_s^2(\omega)g_m^2 < S_{i_d}(\omega)$, which is the typical operating condition, $X_{a,\text{opt}}(\omega)$ and $B_{b,\text{opt}}(\omega)$ become

$$X_{a,\text{opt}}(\omega) = \pm \sqrt{R_s(\omega)(\sqrt{1/\Gamma(\omega)} - R_s(\omega))} \quad (21)$$

$$B_{b,\text{opt}}(\omega) = \pm \sqrt{\frac{\Gamma(\omega)}{R_s(\omega)}(\sqrt{1/\Gamma(\omega)} - R_s(\omega))} - B_c(\omega) \quad (22)$$

where $\Gamma(\omega)$ is the ratio of the uncorrelated gate noise to the normalized drain noise and given by

$$\Gamma(\omega) = \frac{S_{i_{\text{gu}}}(\omega)}{S_{i_d}(\omega)/g_m^2} = \frac{\delta}{5\gamma} \frac{g_m^2}{g_{d0}^2} (1 - |c|^2) (\omega C_{\text{gs}})^2. \quad (23)$$

In (21) and (22), there are two possible optimal matching solutions as indicated by “ \pm ,” both of which yield the same minimum NF.

Reactance $X_{a,\text{opt}}(\omega)$ and susceptance $B_{b,\text{opt}}(\omega)$ given in (19) and (20) [or (21) and (22)] minimize the total output noise by appropriately selecting the voltage gain in the matching network and by exploiting the correlation between $i_g(t)$ and $i_d(t)$. The first operating condition with the corresponding matching network in (19) and (20) represents the condition when $i_{\text{gu}}(t)$ is large relative to $i_d(t)$, i.e., the first term on the right-hand side of (17) is greater than the second term. The optimal solution is then to minimize the effect of $i_{\text{gu}}(t)$ by setting $X_{a,\text{opt}}(\omega) = 0$ and use $B_{b,\text{opt}}(\omega)$ only to exploit the correlation between $i_g(t)$ and $i_d(t)$. However, when $i_d(t)$ is large relative to $i_{\text{gu}}(t)$, which corresponds to the second operating condition, the optimal matching network given in (21) and (22) allows some amplification of $i_{\text{gu}}(t)$ to best exploit the correlation between $i_g(t)$ and $i_d(t)$.

The optimal matching network minimizes the degradation in SNR_{out} caused by the additive noise at every frequency, and hence they become independent of the received signal pulse and the narrow-band interferer. In a realistic matching network with a fixed structure, however, designing $X_a(\omega)$ and $B_b(\omega)$ with arbitrary reactance and susceptance as assumed in the optimum matching network is in general not possible. The matching network then becomes a function of both the transmitted signal pulse and the narrow-band interferer. The suboptimum matching network is described in the following section.

When computing the NF, $S_{v_s}(\omega)$ is, by definition, the PSD of a white thermal noise with noise temperature of 290 K. After de-

terminating the output SNR of the LNA by substituting (19)–(22) into (16), the optimum NF NF_{opt} can be obtained as shown in (24) at the bottom of the page, where $P_T = \int |P(\omega)|^2 d\omega$

$$\Omega_1 = \{ \omega: S_{i_{\text{gu}}}(\omega)R_s^2(\omega)g_m^2 \geq S_{i_d}(\omega), \text{ for } \forall \omega \} \quad (25)$$

$$\Omega_2 = \{ \omega: S_{i_{\text{gu}}}(\omega)R_s^2(\omega)g_m^2 < S_{i_d}(\omega), \text{ for } \forall \omega \} \quad (26)$$

and ω_T is the unity gain angular frequency

$$\omega_T = \frac{g_m}{C_{\text{gs}}} = \frac{3}{4} \frac{v_{\text{sat}}}{L} \frac{(1 + \rho/2)\rho}{(1 + \rho)^2}. \quad (27)$$

The corresponding signal-voltage power gain (in units of V^2/V^2) of the LNA with the optimal matching network, denoted as G_{opt} is

$$\begin{aligned} G_{\text{opt}} &= g_m^2 R_{\text{load}}^2 \\ &\times \int_{-\infty}^{\infty} \frac{1}{(1 - X_{a,\text{opt}}(\omega)B_{b,\text{opt}}(\omega))^2 + (R_s B_{b,\text{opt}}(\omega))^2} \\ &\times \left(\frac{|P(\omega)|^2}{P_T} \right) d\omega. \end{aligned} \quad (28)$$

As will be shown in the following sections, a tradeoff between high G_{opt} and low NF_{opt} exists by varying ρ for a given P_o .

A. Narrow-Band LNA

In a narrow-band LNA, the input signal is assumed to be a single tone when determining the NF. This assumption corresponds to $P(\omega)$ being a nonzero value only when $|\omega| = \omega_0$, where ω_0 is the angular frequency of the single tone. Assuming $S_{i_{\text{gu}}}(\omega_0)R_s^2(\omega_0)g_m^2 < S_{i_d}(\omega_0)$, the optimum NF given in (24) then simplifies to

$$\text{NF}_{\text{opt}} = 1 + \frac{\omega_0}{\omega_T} \sqrt{\frac{4\delta\gamma}{5}(1 - |c|^2)}. \quad (29)$$

The NF equation in (29) is identical to the minimum NF equation calculated for a narrow-band LNA in [8, Ch. 11, eq. (22)]. The corresponding optimum source admittance in [8] can also be obtained based on (21) and (22). As shown in Fig. 3, the equivalent source admittance $Y_{\text{eq}} (= G_{\text{eq}} + jB_{\text{eq}})$ can be written as

$$G_{\text{eq}}(\omega_0) = \frac{R_s(\omega_0)}{R_s^2(\omega_0) + X_{a,\text{opt}}^2(\omega_0)} = \frac{g_m}{g_{d0}} \omega_0 C_{\text{gs}} \sqrt{\frac{\delta}{5\gamma}(1 - |c|^2)} \quad (30)$$

$$\begin{aligned} B_{\text{eq}}(\omega_0) &= B_{b,\text{opt}}(\omega_0) - \omega_0 C_{\text{gs}} - \frac{X_{a,\text{opt}}(\omega_0)}{R_s^2(\omega_0) + X_{a,\text{opt}}^2(\omega_0)} \\ &= \omega_0 C_{\text{gs}} \left(1 + \frac{g_m}{g_{d0}} |c| \sqrt{\frac{\delta}{5\gamma}} \right) \end{aligned} \quad (31)$$

where (30) and (31) are equivalent to the optimum source conductance and susceptance of a narrow-band LNA derived in [8, ch. 11, eqs. (20), (21)]. Hence, when the narrow-band LNA

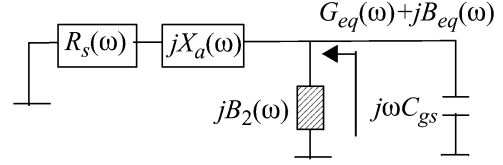


Fig. 3. Equivalent source admittance.

assumption is made, the optimal wideband matching network proposed in this paper simplifies to the published optimum narrow-band matching network. The corresponding NF value is also equivalent.

B. Constant $P(\omega)$

To better understand the effects of the wideband input signal, $P(\omega)$ is assumed to have a brickwall frequency response with a passband $|\omega| \in (\omega_1, \omega_2)$. Assuming $S_{i_{\text{gu}}}(\omega)R_s^2(\omega)g_m^2 < S_{i_d}(\omega)$, the optimum NF given in (24) then becomes

$$\text{NF}_{\text{opt}} = \frac{\lambda \cdot \Delta\omega}{\ln\left(\frac{\lambda\omega_2 + 1}{\lambda\omega_1 + 1}\right)} \quad (32)$$

where $\lambda \triangleq (1/\omega_T) \sqrt{(4\delta\gamma/5)(1 - |c|^2)}$ and $\Delta\omega = \omega_2 - \omega_1$. Making the generally valid assumption that $\lambda\omega_1 \gg 1$, (32) approximates to

$$\text{NF}_{\text{opt}} \approx \frac{\lambda \cdot \Delta\omega}{\ln\left(\frac{\omega_2}{\omega_1}\right)} = \frac{\lambda \cdot \Delta\omega}{\ln\left(1 + \frac{\Delta\omega}{\omega_1}\right)} \quad (33)$$

where (33) shows that the optimum NF is proportional to $\Delta\omega / \ln(1 + \Delta\omega/\omega_1)$. Since the numerator of this ratio increases faster than the denominator as $\Delta\omega$ increases, the achievable NF worsens as the signal bandwidth widens. Hence, the achievable performance of the LNA degrades as the input signal becomes more wideband.

IV. SUBOPTIMAL LNA MATCHING

Since realizing the optimum matching network is in general difficult, a heuristic approach for determining a practical but suboptimum matching network is presented. Based on the frequency responses of $X_{a,\text{opt}}(\omega)$ and $B_{b,\text{opt}}(\omega)$, a structure for the suboptimum matching network that best approximates the optimal responses is first selected. The inductance and capacitance values in the selected structure are then chosen to maximize the SNR_{out} in (16) using numerical optimization techniques. The effectiveness of the suboptimum matching network can be determined by comparing the resulting NF with the lower bound set by NF_{opt} given in (24). A small difference between these two NF values implies that the suboptimum matching network is effective and that it achieves near optimum matching performance. A large difference, however, suggests that a different (and probably more complex) structure for the suboptimum matching network should be chosen.

$$\text{NF}_{\text{opt}} = \frac{1}{\int_{\Omega_1} \frac{1}{1 + \frac{\gamma}{g_m R_s} \frac{g_{d0}}{g_m} + \frac{\delta}{5g_{d0}} \omega^2 C_{\text{gs}}^2} \left(\frac{|P(\omega)|^2}{P_T} \right) d\omega + \int_{\Omega_2} \frac{1}{1 + \frac{\omega}{\omega_T} \sqrt{\frac{4\delta\gamma}{5}(1 - |c|^2)}} \left(\frac{|P(\omega)|^2}{P_T} \right) d\omega} \quad (24)$$

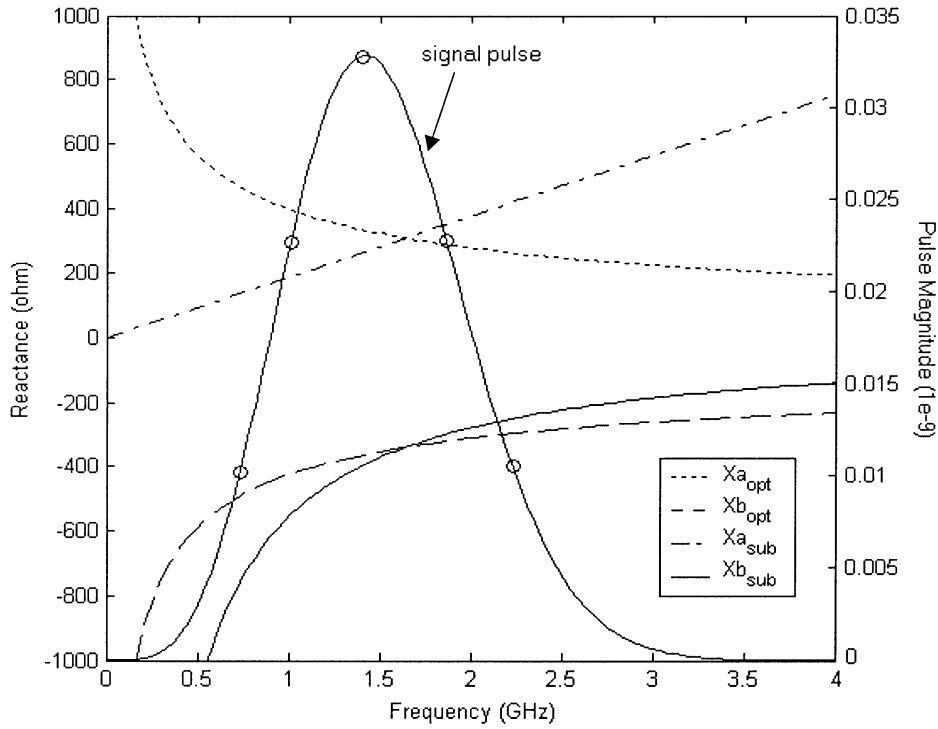


Fig. 4. Suboptimal and optimal reactances when $P_o = 1$ mW and $\rho = 0.1$ ($g_m = 7.7$ mS and $C_{gs} = 104$ fF). For suboptimal matching, $L_a = 29.8$ nH and $C_b = 286$ fF.

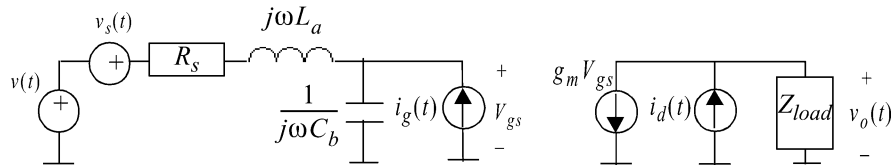


Fig. 5. Suboptimal LNA matching.

To better illustrate the suboptimum matching network design approach, a specific design example is considered. For ease of explanation, the inductors in this example are assumed ideal, although more complex inductor models can also be readily employed. In our example, the source impedance is resistive (i.e., $R_s(\omega) = 50 \Omega$ and $X_s(\omega) = 0$) over the frequency band of interest. As in [18], the received signal pulse is assumed to be a second derivative of a Gaussian pulse, i.e.,

$$p(t) = \sqrt{\frac{4}{3\sigma\sqrt{\pi}}} \left(1 - \left[\frac{t}{\sigma}\right]^2\right) \exp\left(-\frac{1}{2}\left[\frac{t}{\sigma}\right]^2\right) \quad (34)$$

where σ is the standard deviation of the Gaussian pulse. Its corresponding Fourier transform is

$$P(\omega) = \sqrt{\frac{4\sigma\sqrt{\pi}}{3}} [\sigma\omega]^2 \exp\left(-\frac{1}{2}[\sigma\omega]^2\right). \quad (35)$$

Reactances $X_a(\omega)$ and $X_b(\omega) (= -1/B_b(\omega))$ for both the optimum and the suboptimum matching networks are shown in Fig. 4. A plot of the transmit signal pulse is also shown for reference. The operating conditions are assumed to be $\sigma = 0.1592$ ns, $g_m = .7.7$ mS, and $C_{gs} = 1$ pF. To realize the suboptimum matching network, $X_{a,opt}(\omega)$ is approximated using an inductor and $X_{b,opt}(\omega)$ using a capacitor. A circuit model of the suboptimum matching network is shown in Fig. 5, and the resulting

frequency response of the optimum and suboptimum matching network is plotted in Fig. 6. The reactance $X_a(\omega)$ and susceptance $B_b(\omega)$ of the suboptimum matching network with inductance L_m and capacitance C_m are $j\omega L_a$ and $j\omega C_b$, respectively, where $C_b = C_{gs} + C_m$ and $L_a = L_m$. The choice of L_a and C_b is determined by solving the following constrained optimization problem:

$$\begin{aligned} \text{minimize} \quad \text{NF} &= \frac{1}{\int_{-\infty}^{\infty} \frac{1}{1+F_1(\omega)+F_2(\omega)} \left(\frac{|P(\omega)|^2}{P_T}\right) d\omega} \quad (36) \\ \text{subject to} \quad L_a &\geq 0, \quad C_b \geq C_{gs} \quad (37) \end{aligned}$$

where $F_1(\omega)$ is the contribution due to the uncorrelated gate noise $i_{gu}(t)$, and $F_2(\omega)$ is the contribution due to the drain noise $i_d(t)$ and the component of the gate correlated to $i_d(t)$, i.e.,

$$\begin{aligned} F_1(\omega) &= \frac{\delta}{5g_m R_s g_{d0}} (1 - |c|^2) \omega^2 C_{gs}^2 [R_s^2 + (\omega L_a)^2] \quad (38) \\ F_2(\omega) &= \frac{\gamma}{g_m R_s g_m} \left\{ R_s^2 \omega^2 \left[C_b + C_{gs} \left(\frac{g_m |c| \sqrt{\frac{\delta}{5\gamma}}}{g_{d0}} \right) \right]^2 \right. \\ &\quad \left. + \left[1 - \omega^2 L_a \left(C_b + C_{gs} \left(\frac{g_m |c| \sqrt{\frac{\delta}{5\gamma}}}{g_{d0}} \right) \right) \right]^2 \right\}. \quad (39) \end{aligned}$$

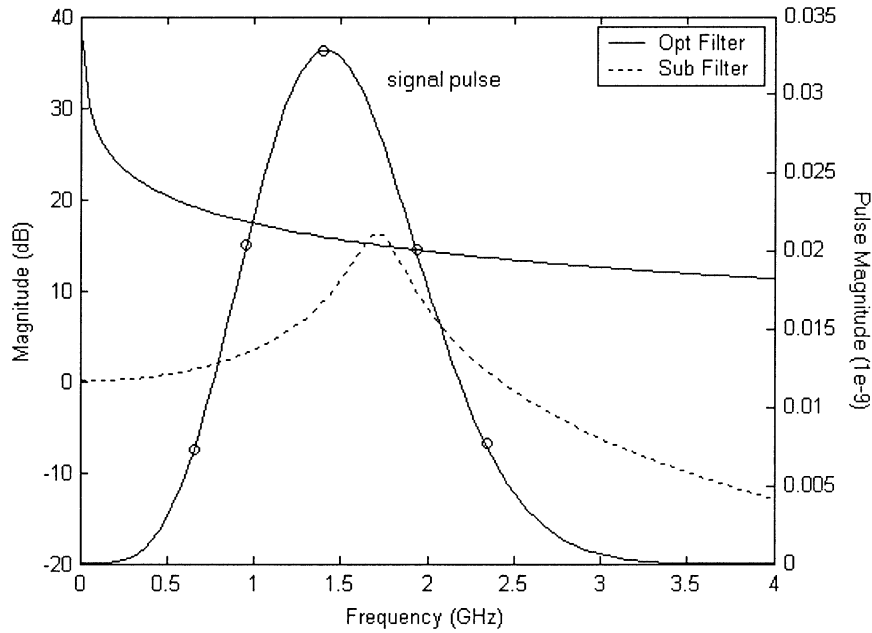


Fig. 6. Magnitude response of the suboptimal and optimal matching network when $P_o = 1$ mW and $\rho = 0.1$ ($g_m = 7.7$ mS and $C_{gs} = 104$ fF). For suboptimal matching, $L_a = 29.8$ nH, and $C_b = 286$ fF.

The corresponding signal voltage power gain (in units of V^2/V^2) is

$$G = g_m^2 R_{\text{load}}^2 \int_{-\infty}^{\infty} \frac{1}{(1 - \omega^2 L_a C_b)^2 + (\omega R_s C_b)^2} \left(\frac{|P(\omega)|^2}{P_T} \right) d\omega. \quad (40)$$

In the above constrained optimization problem, the values for L_a and C_b that minimize NF in (36) can be solved by approximating the integral by finite summation and using numerical iterative search techniques such as the sequential quadratic programming (SQP) method [19]. To prevent convergence to a local minimum using these iterative search methods, the initial guesses for L_a and C_b must be sufficiently close to their optimal values. A good initial guess can be obtained by choosing L_a and C_b values that accurately approximate the optimal reactances over the signal frequency band.

V. RESULTS AND DISCUSSIONS

A. Parameter Extraction

The performance results presented in this section are for the design example given in Section IV. The parameters for the transistor model in Section II-A are obtained using the Y -parameter analysis technique [20] with BsimV3V model and the Cadence SpectreRF simulator. For $L = 0.24$ μm and $V_{\text{supply}} = 2.5$ V, the following transistor parameters were extracted: $v_{\text{sat}} = 73.6$ Km/s, $\epsilon_{\text{sat}} = 4.96$ MV/m, and $C_{\text{ox}} = 7.3$ mF/m². Fig. 7(a)–(c) shows the drain current I_d , the transconductance g_m , and the zero-bias drain conductance g_{d0} obtained from SpectreRF (represented by dots) along with the corresponding curves obtained by using the extracted parameters with (1), (6), and (7). A close agreement between simulation and the equations using the extracted parameters is observed.

Parameters γ , δ , and c used to characterize the transistor noise in Section II-B cannot be determined using SpectreRF, since the induced gate noise is not modeled. Hence, these parameters are obtained based on the experimentally measured two-port noise parameters for selected transistor sizes and operating conditions. Parameters γ , δ , and c are extracted using the noise de-embedding technique described in [21]. The resulting values are $\gamma = 1.0$, $\delta = 4.0$, and $c = 0.98$ j. Fig. 8(a)–(c) shows the drain noise $i_d(t)$, the induced gate current noise $i_g(t)$, and their cross-correlation coefficient c as a function of frequency. The dots represent the experimentally measured values and the curves represent the estimates using (10), (11), and (12) with extracted parameters. A close agreement is again observed between the dots and the curves.

B. Performance Results

The performance results are obtained using the extracted parameters described in the previous subsection. The source and load impedance are assumed resistive, i.e., $Z_s(\omega) = Z_{\text{load}}(\omega) = 50$ Ω . The received signal pulse is the second derivative of a Gaussian pulse given in (34) with σ of 0.1592 ns unless stated otherwise.

Fig. 9(a) plots the NF as a function of the normalized gate overdrive ρ for different power dissipation P_o values. The corresponding signal voltage gain G (in units of V^2/V^2) for the same operating conditions is shown in Fig. 9(b). The NF curves are obtained using (24) for the optimum and (36) for the suboptimum matching networks and by replacing all occurrences of g_m and C_{gs} with ρ and P_o [using (6) and (8)]. The optimum NF monotonically decreases and converges to an asymptotic value with increasing ρ . In the suboptimum matching network, however, there is an optimum ρ that minimizes the NF for a given P_o . The gap between the minimum NF of the suboptimum matching network and the optimum NF narrows with increasing

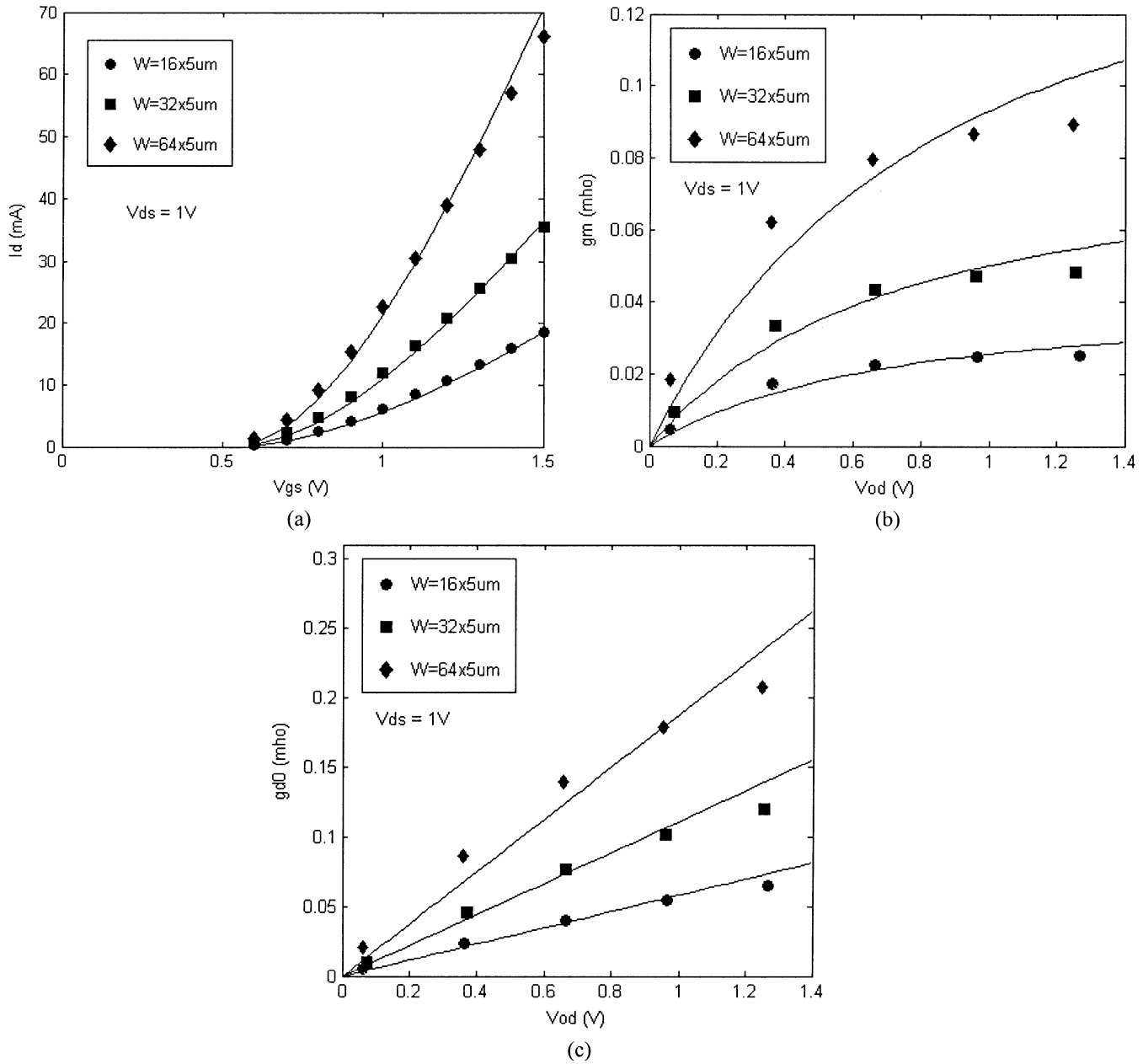


Fig. 7. Comparisons between the simplified MOS model in Section II-A and BsimV3V for the n-type MOSFETs with channel length of $L = 0.24 \mu\text{m}$ and different widths of $W = 16 \times 5$, 32×5 , and $64 \times 5 \mu\text{m}$, all biased at $V_{ds} = 1 \text{ V}$. Dots are obtained using SpectreRF. Curves are based on extracted transistor parameters. (a) Drain current I_d versus gate overdrive voltage V_{od} . (b) Transconductance g_m versus gate overdrive voltage V_{od} . (c) Zero-bias drain conductance g_{d0} versus gate overdrive voltage V_{od} .

P_o . For example, when $P_o = 10 \text{ mW}$, the NF of the suboptimum matching network becomes approximately 1 dB greater than that of the optimum NF. This gap can be further reduced by increasing P_o and/or employing more sophisticated matching network than the simple inductor and capacitor employed in Fig. 5. The G curves for the optimum and suboptimum matching networks are obtained using (28) and (40), respectively. For both matching networks, G increases with P_o . A maximum G exists for the suboptimum matching network.

In Fig. 10, the NF is plotted against G of both the optimum (dash line) and the suboptimum matching networks (solid line) by fixing P_o and varying ρ . The region in the upper left corner of Fig. 10 represents the NF and G values corresponding to small

ρ values. For the optimum matching network, the NF decreases monotonically [as in Fig. 9(a)] whereas G peaks then drops with increasing ρ . The peaking occurs because the two gain components of G change in opposite directions with increasing ρ : the voltage gain in the matching network increases but g_m of the transistor decreases [see (6)]. The suboptimum matching network behaves similarly to the optimum matching network, except that the NF does not decrease monotonically. This results because there is an optimum ρ that minimizes the NF as shown in Fig. 9(a). Fig. 10 suggests that this optimum ρ also approximately maximizes G .

In Fig. 11, the NF and G of the suboptimal matching LNA are plotted as a function of σ . Although the advantages of the

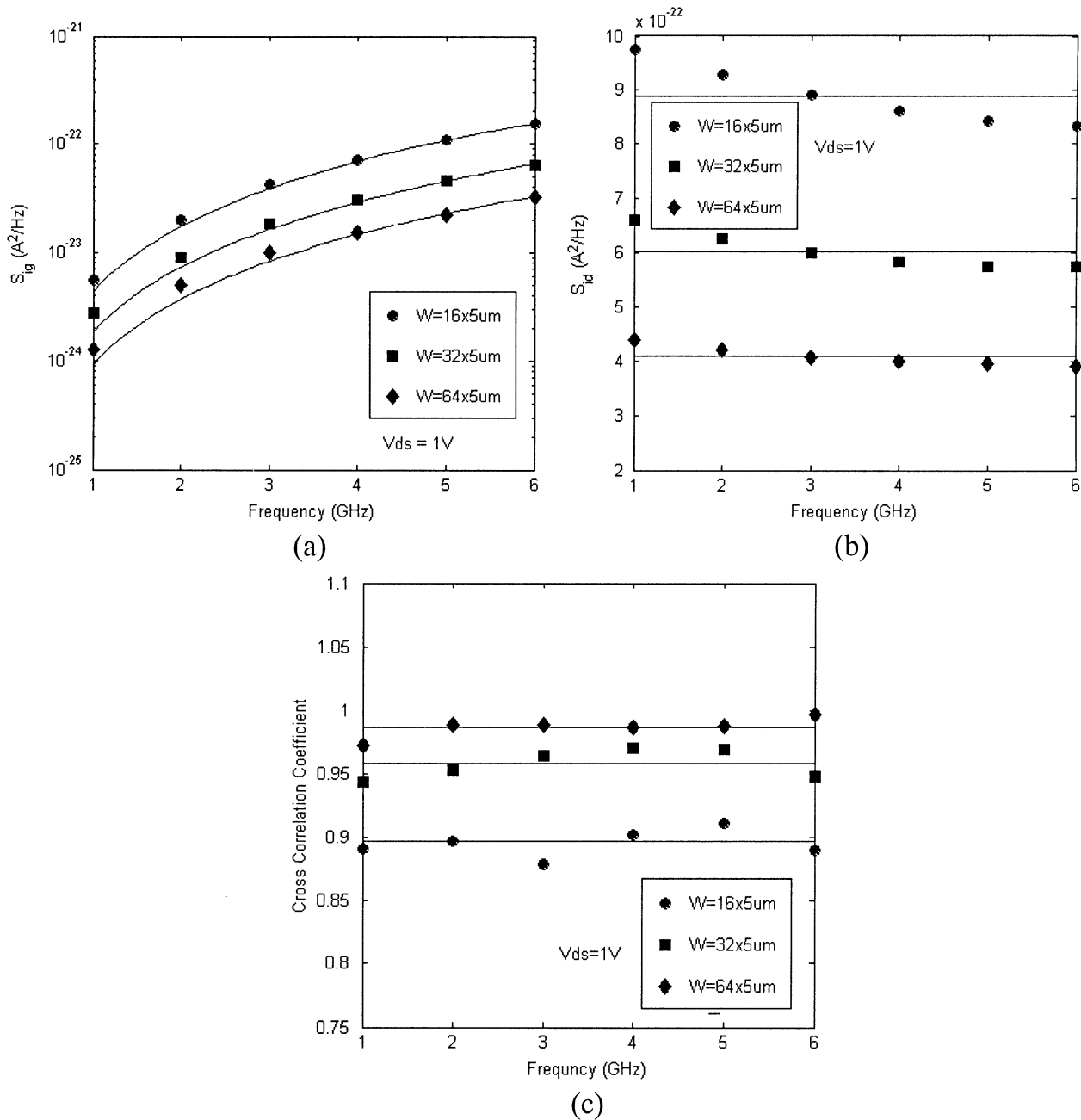


Fig. 8. Comparison between the device noise PSD obtained from measured two-port noise parameters and from extracted γ , δ , and c values for n-type MOSFETs of channel lengths $L = 0.24 \mu\text{m}$ and widths of $W = 16 \times 5$, 32×5 , and $64 \times 5 \mu\text{m}$, all biased at $V_{ds} = 1\text{V}$. Dots are obtained using measured two-port noise parameters. Curves are obtained using equations in Section II-B with extracted parameters. (a) Induced gate noise versus frequency. (b) Drain channel noise versus frequency. (c) Cross-correlation coefficient versus frequency.

UWB radio described in Section I generally improves with narrower pulsewidth (or increased signal bandwidth), both the NF and G of the LNA worsen. This degradation in NF occurs because as the pulsewidth narrows, the signal spectra widens and a greater percentage of the signal spectra falls in the higher frequency region where $i_g(t)$ with its PSD proportional to ω^2 becomes more significant. Since the voltage gain of the matching network must also be reduced to minimize NF, the overall gain G is correspondingly degraded. The effect of $i_g(t)$ on both the NF and G can be improved by increasing P_o as shown in Fig. 11. Increasing P_o results in higher g_m [see (6)]

and also shifts the induced gate noise [$S_{i_g}(\omega)$ in (11)] upwards in frequency.

C. Narrow-Band Interferer

The UWB radio must coexist with many narrow-band radio systems located within its signal bandwidth. Ideally, the design of the LNA in the UWB radio should be optimized to account for the effect of these narrow-band radio systems, which can be modeled as narrow-band interferers. In practice, however, the spectrum of these interferers are not known a priori, making such optimization at design time difficult. The effectiveness of

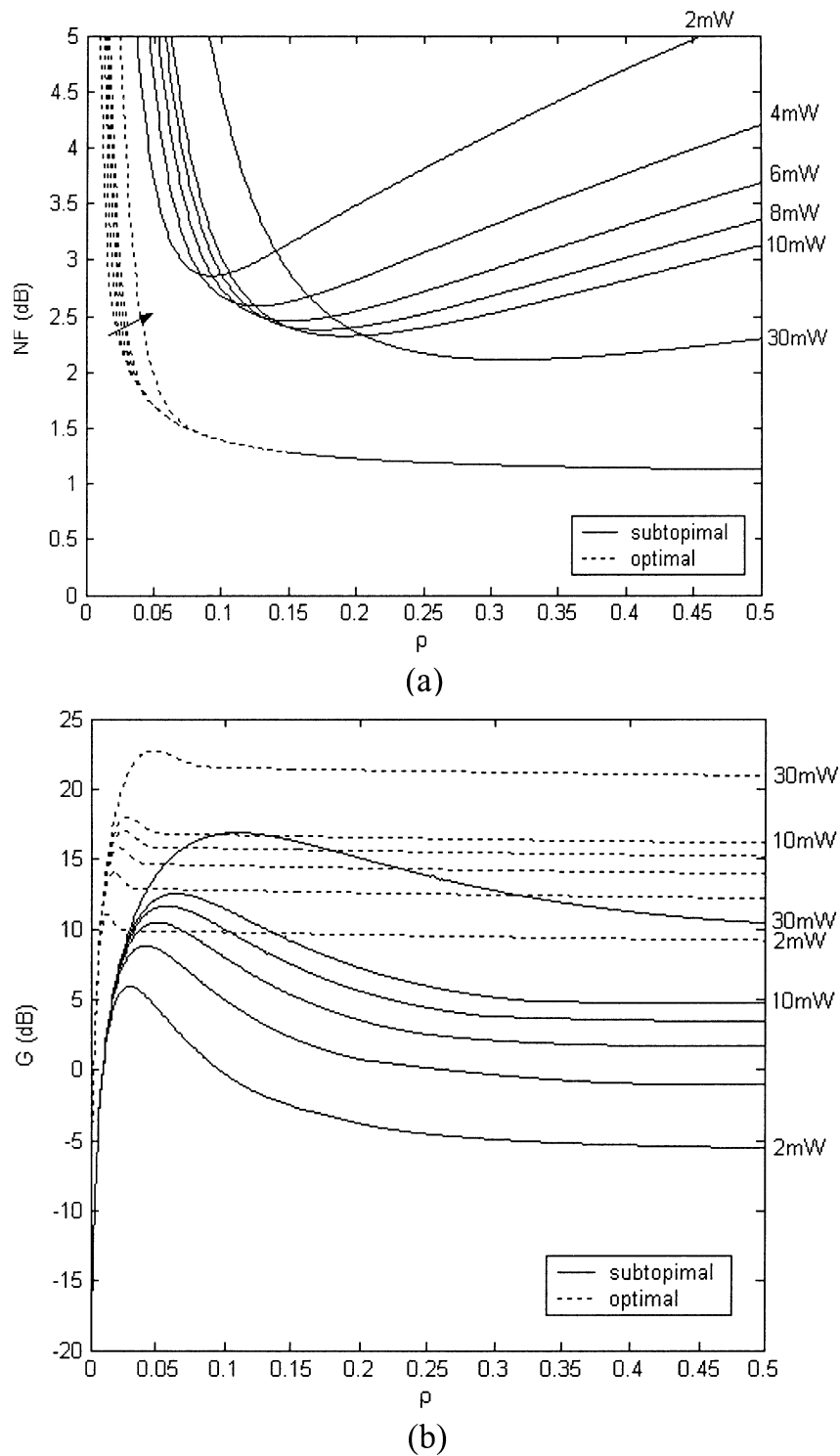


Fig. 9. Contours of suboptimal (solid line) and optimal (dash line) curve as a function of the normalized gate overdrive (ρ) with P_o ranging from 2 to 10 mW (increasing P_o in the direction of the arrow) (a) NF. (b) Gain.

the proposed LNA matching network, therefore, depends on its sensitivity to these narrow-band interferers. We quantify this sensitivity by computing the degradation in the output SNR relative to the input SNR of an LNA designed assuming no interferer is present (when an interferer is in fact present) to an LNA designed with perfect knowledge of the interferer spectrum $S_I(\omega)$. For ease of explanation, we subsequently refer to the former

LNA as the “approximate” LNA and the latter LNA as the “accurate” LNA. Since the optimum matching network given in (19)–(22) is independent of the interferer spectrum $S_I(\omega)$ as described earlier, only the suboptimum matching network is considered.

The narrow-band interferer is assumed to have a brickwall spectrum that is 50 dB greater than the input noise floor. For

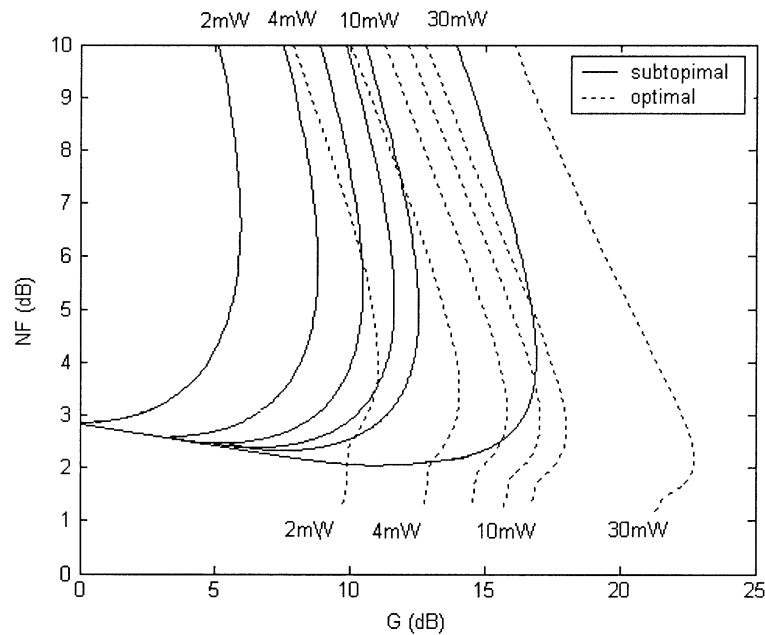


Fig. 10. Contours of NF and signal gain obtained by fixing P_o and varying ρ for optimal (dash line) and suboptimal (solid line) matching.

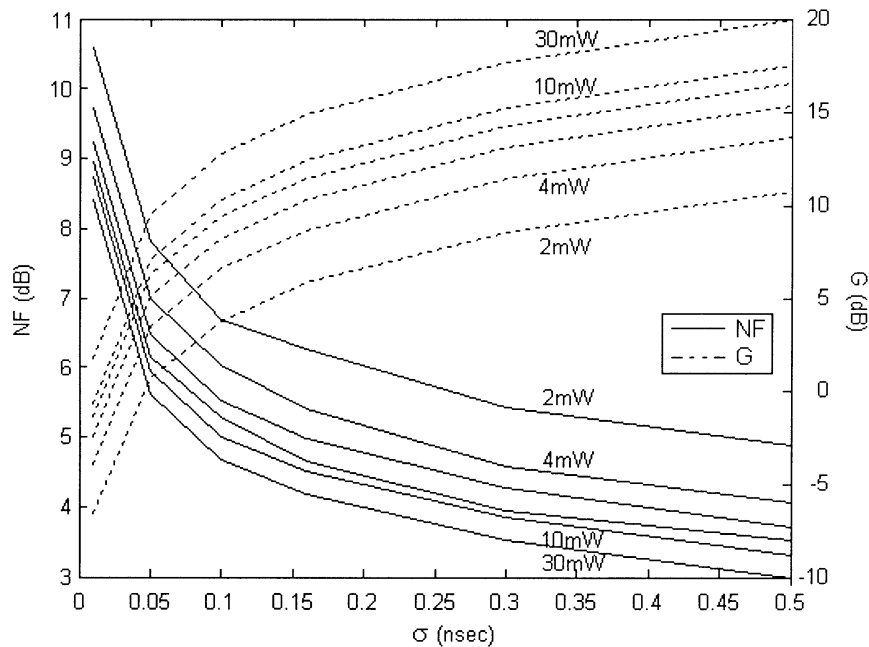


Fig. 11. Contours of the NF (solid line) and signal gain (dash line) as a function of pulsewidth for suboptimal matching.

worst case analysis, we assume that the interferer is centered at the frequency corresponding to the peak of the received signal spectrum. In Fig. 12, the loss in SNR of both the approximate and accurate LNA is plotted as a function of the gate overdrive ρ for different P_o values. The bandwidth of the interferer is assumed to be 10% of the bandwidth of the Gaussian transmitted pulse, which is defined as the frequency band within which 90% of the signal energy is contained. The difference in NF between the approximate and accurate LNA depends on ρ . Since the receiver has no a priori knowledge of the interferer, ρ of the approximate LNA should be set to minimize the NF when no interferer is present (see Fig. 9). The approximate LNA then suffers less than 0.2 dB compared to the accurate LNA. This small

degradation in performance of the approximate LNA is not surprising since the suboptimal matching network approximates the optimum matching network, which is independent of the interferer. The gap between the two LNAs in Fig. 12 can be further reduced by employing a matching network structure that better approximates the optimal matching network.

D. Design Example

A design example of an LNA with suboptimal matching network is described when the power consumption is constrained to be 8 mW and the equivalent pulse response $P(\omega)$ is a second derivative of the Gaussian pulse with $\sigma = 0.1592$ ns. From

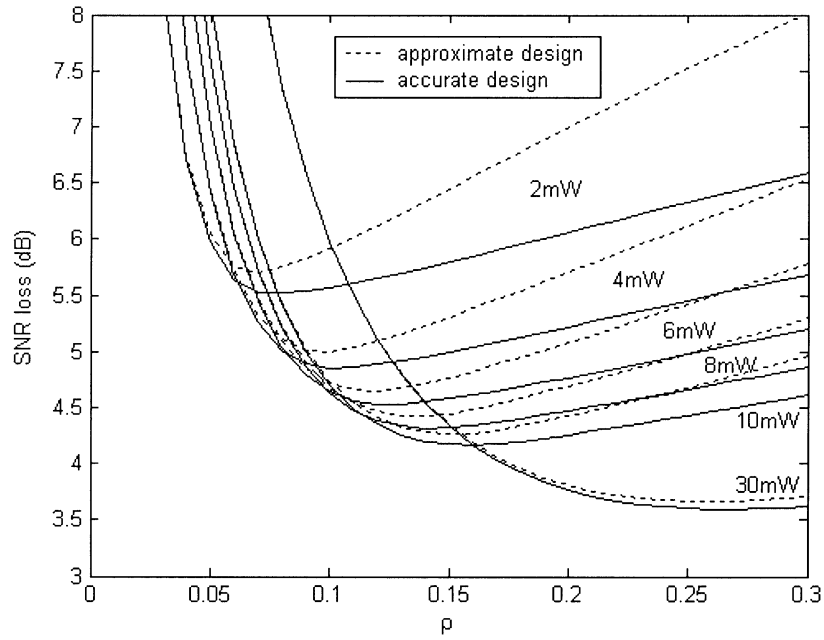


Fig. 12. Contours of SNR loss for approximate and accurate LNA.

TABLE I
LNA NOISE MATCHING DESIGN EXAMPLE WITH POWER CONSTRAINT OF $P_o = 8$ mW

Design Type	Design Parameters	Value
MOS Transistor	Width (μm)	64x5
	V_{gs} (mV)	715
	Computed g_m (mS)	56.1
	Simulated g_m (mS)	50.5
Narrowband Matching Network	L_a (nH)	4.5
	C_b (fF)	914
	Computed G (dB)	11.38
	Simulated G (dB)	10.87
Suboptimal Wideband Matching Network	L_a (nH)	3.2
	C_b (fF)	914
	Computed G (dB)	10.29
	Simulated G (dB)	9.75
Optimal Wideband Matching Network	Computed G (dB)	15.1
	NF (dB)	1.4

Note: Computed value of g_m and G are based on (6) and (4). Simulations are also carried out with Bsim V3V model using Cadence SpectreRF. NFs are calculated using parameters γ , δ , and c that were extracted from experimentally measured noise parameters.

Fig. 9(a) and (b), the minimum NF is obtained when $\rho = 0.2$ and the maximum voltage gain when $\rho = 0.05$. As a compromise between voltage gain and NF, we choose ρ to be 0.1. The gate bias voltage is determined using the definition of ρ . The transistor width is also readily specified given ρ and P_o from (8), and it is $320 \mu\text{m}$, which we realized using 64 finger each of width $5 \mu\text{m}$. Given the width and bias of the transistor, the suboptimal matching network is determined by solving the constrained optimization problem in (36)–(37). The design parameters and the results are summarized in Table I. For comparison purposes, the performance of an LNA with optimum matching

network and a narrow-band LNA are also included in the table. The narrow-band LNA is designed by solving the constrained optimization problem in (36)–(37) assuming is a single-tone pulse centered at 1.42 GHz, which corresponds to the peak of the second derivative of the UWB Gaussian pulse.

VI. CONCLUSION

In contrast to narrow-band systems, the use of the NF performance metric becomes problematic in UWB systems because of the difficulty in defining the SNR. For the NF of the LNA

to be a meaningful metric in an UWB receiver, the SNR should measure the achievable performance after the eventual digital decoding process, as it is ultimately the most relevant measure of performance. Hence, the SNR is defined as the MFB, which represents an upper limit on the performance of data transmission systems. By defining the SNR as the MFB, the NF measures the degree of degradation in the achievable receiver performance caused by the LNA.

Using the above definition of NF, a general approach for designing an UWB LNA that minimizes the NF has been developed. Minimizing the NF is equivalent to maximizing the output SNR, since the input SNR is unaffected by the matching network. The matching network consists of two lossless reactances, which are connected in series and in parallel to the MOS amplifier. The optimum matching network that minimizes the NF with the SNR defined as the MFB has been solved. When the input is assumed to be a single tone, the proposed optimum matching network simplifies to the published optimum matching network of a narrow-band LNA. The corresponding NF value also becomes equivalent. Since realizing the optimum matching network is in general difficult, a heuristic approach for designing a practical but suboptimum matching network is also presented. The performance of a simple suboptimum matching network consisting of an inductor in series and a capacitor in parallel to the MOS amplifier is evaluated. Although this simple suboptimum matching network performs reasonably well, the performance can be further improved by employing a different and probably more complex structure that better approximates the optimum matching network.

REFERENCES

- [1] M. Z. Win and R. A. Scholtz, "Impulse radio: How it works," *IEEE Commun. Lett.*, vol. 2, pp. 36–38, Feb. 1998.
- [2] —, "Comparisons of analog and digital impulse radio for multiple-access communications," in *Proc. IEEE Int. Conf. on Commun.*, vol. 1, Montreal, Canada, June 1997, pp. 91–95.
- [3] S. S. Kolenchery, J. K. Townsend, and J. A. Freebersyser, "A novel impulse radio network for military communications," in *Proc. Military Comm. Conf.*, vol. 1, Boston, MA, Oct. 1998, pp. 59–65.
- [4] M. Z. Win and R. A. Scholtz, "On the robustness of ultrawide bandwidth signals in dense multipath environments," *IEEE Commun. Lett.*, vol. 2, pp. 51–53, Feb. 1998.
- [5] —, "Ultra-wide bandwidth signal propagation for indoor wireless communications," in *Proc. Int. Conf. Commun.*, Montreal, Canada, June 1997.
- [6] D. K. Shaeffer and T. H. Lee, "A 1.5-V, 1.5-Hz CMOS low-noise amplifier," *IEEE J. Solid-State Circuits*, vol. 32, pp. 745–759, May 1997.
- [7] H. A. Haus, "IRE standards on methods of measuring noise in linear two ports, 1959," *Proc. IRE*, vol. 48, pp. 60–74, 1960.
- [8] T. H. Lee, *The Design of CMOS Radio-Frequency Integrated Circuits*. Cambridge, U.K.: Cambridge Univ. Press, 1998.
- [9] J. G. Proakis, *Digital Communications*. Boston, MA: McGraw-Hill, 2001.

- [10] C. G. Sodini, P.-K. Ko, and J. L. Moll, "The effect of high fields on MOS device and circuit performance," *IEEE Trans. Electron Devices*, vol. ED-31, pp. 1386–1393, Oct. 1984.
- [11] N. G. Einspruch, *VLSI Electronics: Microstructure Science*. New York: Academic, 1989, vol. 18, ch. 1, pp. 1–37.
- [12] D. P. Triantis, A. N. Birbas, and D. Kondis, "Thermal noise modeling for short-channel MOSFETs," *IEEE Trans. Electron Devices*, vol. 43, pp. 1950–1955, Nov. 1996.
- [13] P. Klein, "An analytical thermal noise model of deep submicron MOSFETs," *IEEE Electron Device Lett.*, vol. 20, pp. 399–401, Aug. 1999.
- [14] G. Knoblinger, P. Klein, and M. Tiebout, "A new model for thermal channel noise of deep submicron MOSFETs and its application in RF-CMOS design," in *Proc. Symp. VLSI Circuits Dig. Technical Papers*, June 2000, paper 11–14.
- [15] A. van der Ziel, *Noise in Solid State Devices and Circuits*. New York: Wiley, 1986.
- [16] A. Abidi, "High frequency noise measurements on FETs with small dimensions," *IEEE Trans. Electron. Devices*, vol. ED-33, pp. 1801–1805, Nov. 1986.
- [17] D. P. Triantis, A. N. Birbas, and S. E. Plevridis, "Induced gate noise in mosfets revisited: The submicron case," *Solid-State Electron.*, vol. 41, no. 12, pp. 1937–1942, 1997.
- [18] E. A. Homier and R. A. Scholtz, "Rapid acquisition of ultra-wideband signals in the dense multipath channel," in *Proc. IEEE Conf. Ultra Wideband Systems and Technologies*, May 2002, pp. 105–110.
- [19] D. Goldfarb, "A family of variable metric updates derived by variational means," *Math. Comput.*, vol. 24, pp. 23–26, 1970.
- [20] C. C. Enz and Y. Cheng, "MOS transistor modeling for RF IC design," *IEEE J. Solid-State Circuits*, vol. 35, pp. 186–201, Feb. 2000.
- [21] R. A. Pucel, W. Struble, R. Hallgren, and U. L. Rohde, "A general noise de-embedding procedure for packaged two-port linear active devices," *IEEE Trans. Microwave Theory Tech.*, vol. 40, pp. 2013–2024, Nov. 1992.



Jongrit Lerdworatawee (S'03) received the B.Eng. degree from Tsinghua University, Beijing, China, and M.Eng. degree from National University of Singapore, in 1998 and 2000, respectively. He is currently working toward the Ph.D degree at University of Southern California, Los Angeles.



Won Namgoong received the B.S. degree in electrical engineering and computer science from the University of California at Berkeley, and the M.S. and Ph.D degrees in electrical engineering from Stanford University, Stanford, CA, in 1993, 1995, and 1999, respectively.

In 1999, he joined the faculty of the Electrical Engineering Systems Department, University of Southern California, Los Angeles, where he is an Assistant Professor. His current research activities include signal processing systems, wireless communication, and RF/mixed signal circuits and systems.

Dr. Namgoong received the National Science Foundation (NSF) CAREER Award in 2002.